The Astrophysical Journal, 910:134 (19pp), 2021 April 1 https://doi.org/10.3847/1538-4357/abe547

Surveying the X-Ray Behavior of Novae as They Emit γ-Rays

A. C. Gordon[1,2], E. Aydi[1], K. L. Page[3], Kwan-Lok Li[4], L. Chomiuk[1], K. V. Sokolovsky[1], K. Mukai[5,6], and J. Seitz[1]

[1] Center for Data Intensive and Time Domain Astronomy, Department of Physics and Astronomy, Michigan State University, East Lansing, MI 48824, USA muethela@msu.edu
[2] Center for Interdisciplinary Exploration and Research in Astrophysics and Department of Physics and Astronomy, Northwestern University, 2145 Sheridan Road, Evanston, IL 60208-3112, USA; aydielia@pa.msu.edu
[3] School of Physics and Astronomy, University of Leicester, University Road, Leicester, LE1 7RH, UK
[4] Department of Physics, National Cheng Kung University, 70101 Tainan, Taiwan
[5] Center for Space Science and Technology, University of Maryland Baltimore County, Baltimore, MD 21250, USA
[6] CRESST and X-ray Astrophysics Laboratory, NASA/GSFC, Greenbelt, MD 20771, USA
Received 2020 October 29; revised 2021 February 2; accepted 2021 February 2; published 2021 April 5

Abstract

The detection of GeV γ-ray emission from Galactic novae by the Fermi-Large Area Telescope has become routine since 2010, and is generally associated with shocks internal to the nova ejecta. These shocks are also expected to heat plasma to $\sim 10^7$ K, resulting in detectable X-ray emission. In this paper, we investigate 13 γ-ray emitting novae observed with the Neil Gehrels Swift Observatory, searching for 1–10 keV X-ray emission concurrent with γ-ray detections. We also analyze γ-ray observations of novae V407 Lup (2016) and V357 Mus (2018). We find that most novae do eventually show X-ray evidence of hot shocked plasma, but not until the γ-rays have faded below detectability. We suggest that the delayed rise of the X-ray emission is due to large absorbing columns and/or X-ray suppression by corrugated shock fronts. The only nova in our sample with a concurrent X-ray/γ-ray detection is also the only embedded nova (V407 Cyg). This exception supports a scenario where novae with giant companions produce shocks with external circumbinary material and are characterized by lower density environments, in comparison with novae with dwarf companions where shocks occur internal to the dense ejecta.

Unified Astronomy Thesaurus concepts: Classical novae (251); Novae (1127); X-ray astronomy (1810); Cataclysmic variable stars (203); White dwarf stars (1799); Gamma-ray astronomy (628); Gamma-ray transient sources (1853); Symbiotic binary stars (1674); High energy astrophysics (739); Observational astronomy (1145); Shocks (2086)

Supporting material: data behind figures

1. Introduction

A classical nova is a transient event involving an accreting white dwarf in a binary star system (e.g., Bode & Evans 2008). Once the pressure and temperature at the base of the accreted envelope reach a critical level, a thermonuclear runaway is triggered on the surface of the white dwarf, leading to the ejection of at least part of the envelope. Typically, 10^{-7}–10^{-4} $M_\odot$ of the material is ejected at velocities ranging between 500 and 5000 km s^{-1} (e.g., Payne-Gaposchkin 1957; Gallagher & Starrfield 1978; Yaron et al. 2005). Remnants of the accreted envelope remain on the white dwarf's surface and continue nuclear burning for weeks to years after the thermonuclear runaway ends, bathing the ejecta with luminous ionizing radiation from within ($\sim 10^{38}$ erg s^{-1}; Wolf et al. 2013). Early in the nova's evolution, the ejecta are optically thick, and as the thermal emission from the white dwarf diffuses through the ejecta, the nova's spectral energy distribution peaks in the optical band. As the ejecta expand, their density drops, they become more optically thin, and the peak of the nova's spectral energy distribution moves blueward (Gallagher & Code 1974). When the white dwarf is finally reveal to years, until the residual fuel is all burnt (Krautter 2008; Schwarz et al. 2011; Page & Osborne 2014; Osborne 2015). After a period of time, accretion will resume and the process restarts. All novae are theorized to recur, but some novae have been observed to erupt more than once during our observational records; these are known as recurrent novae.

The discovery of GeV γ-rays from nova V407 Cyg with the Large Area Telescope (LAT) on the Fermi Gamma-Ray Space Telescope (henceforth Fermi) has opened the door for a whole new realm of nova research (Abdo et al. 2010). At first, the γ-rays were thought to be the result of the ejecta interacting with the dense wind of V407 Cyg's Mira giant companion, and not a feature of typical nova systems (e.g., Munari et al. 2011; Nelson et al. 2012). However, the discovery of γ-rays from V959 Mon, V1324 Sco, and V339 Del with Fermi-LAT in the following years revealed that V407 Cyg was not a singular case (Ackermann et al. 2014). Unlike V407 Cyg, these systems contain main-sequence companions, so the γ-rays could not be coming from the ejecta interacting with a dense circumbinary medium.

Since 2013, even more novae with main-sequence companions have been detected in the GeV γ-ray band. These observations reveal that shocks are common in nova eruptions and that they are energetically important (Li et al. 2017b; Aydi et al. 2020b). As the majority of Fermi-detected novae have dwarf (rather than giant) companions and low-density circumbinary material, the γ-ray emitting shocks must be internal to the nova ejecta. From high-resolution radio imaging of the nova V959 Mon, it was found that these shocks may occur at the interface between a slow, dense, equatorial torus and a fast biconical wind (Chomiuk et al. 2014). The shocks produced at these interfaces accelerate particles to relativistic speeds via the diffusive shock mechanism and lead to GeV γ-ray emission

(Metzger et al. 2015). These internal shocks have velocities $\sim$1000 km s^{-1}, and consequently heat the post-shock gas to temperatures of $\sim 10^7$ K, which emits relatively hard ($\gtrsim$1 keV; compared to the supersoft component) X-rays. Even before γ-rays were detected in novae, hard X-ray emission was observed and interpreted as an indication of shock interaction (e.g., Mukai & Ishida 2001; Mukai et al. 2008).

In the last two decades, the X-ray Telescope (XRT; Burrows et al. 2005) on the Neil Gehrels Swift Observatory (hereafter Swift; Gehrels et al. 2004) has been instrumental in providing observations for novae in the 0.3–10 keV band at relatively high cadence (e.g., Page et al. 2020a). For example, V407 Cyg showed hard X-ray emission during its first months of evolution concurrent with the γ-ray producing phase; as with the γ-rays, this is likely a result of the nova ejecta interacting with the secondary's wind (Abdo et al. 2010; Nelson et al. 2012; Orlando & Drake 2012).

The hard X-ray behavior of classical novae with main-sequence companions is less clear, especially while γ-rays are being detected. Swift observed V1324 Sco while GeV γ-rays were detected, but failed to detect any X-rays (Finzell et al. 2018). Based on this non-detection, Metzger et al. (2014) theorized that the X-ray emission from classical novae during the γ-ray period would be absorbed by the initially dense ejecta. These absorbed X-rays are then reprocessed and reemitted as UV and optical photons, contributing to the luminosity in those bands (supporting this hypothesis, correlated γ-ray and optical light curves have been observed in two novae to date; Li et al. 2017b; Aydi et al. 2020b). Once the ejecta expand enough and the optical depth decreases, X-rays are allowed through.

Similar to V1324 Sco, there are hints from other novae that 1–10 keV X-rays were not detectable by Swift until $\gtrsim$1 month after eruption (e.g., Shore et al. 2016; Mason et al. 2018), but the X-ray light curves were not explicitly discussed in the context of γ-rays and shocks. Interestingly, harder X-rays (>10 keV) from novae have begun to be detected with NuSTAR concurrent with γ-rays (Nelson et al. 2019; Aydi et al. 2020b; Sokolovsky et al. 2020b), but at surprisingly low fluxes (the implications of these observations will be discussed in Section 4). Despite the rapid response and agility of Swift that make it ideal for observations during the early weeks of nova eruptions (when novae are bright in GeV γ-rays), no systematic study has been carried out of Swift-XRT observations of γ-ray detected novae. It is the goal of this paper to test if all classical novae are faint in the 1–10 keV X-ray band during γ-ray detection.

Previous studies have been carried out on large collections of novae in the supersoft X-ray phase using observations from Swift-XRT, including those of Ness et al. (2007), Schwarz et al. (2011), and Page et al. (2020a). However, systematic studies of the harder X-ray component, or the X-ray behavior of γ-ray detected novae, are lacking. In this paper, we present a systematic study of 13 Galactic novae that have been detected by Fermi-LAT between 2010 and 2018 and have been observed by Swift-XRT. In Section 2, we discuss the sample selection and the multiwavelength properties of the novae in our sample. Fermi-LAT data for most novae in our sample have already been published, but we present the first γ-ray analysis of novae V407 Lup and V357 Mus. In Section 3, we present the Swift-XRT observations, emphasizing the hard X-ray emission during the γ-ray detection phase. In Section 4, we discuss what can be learned about nova shocks from observations concurrent with γ-rays, and in Section 5 we conclude.

2. Our Sample of γ-Ray Detected Novae

2.1. Sample Selection

In this paper, we analyze all Galactic novae observed by Fermi-LAT between 2010 and 2018 that have a time-integrated detection of $\geqslant 3\sigma$ significance over the period of γ-ray emission. Details of the sample are listed in Table 1. Despite hints that they produced γ-ray emission, we do not include novae V745 Sco, V697 Car, or V1535 Sco in our sample because their Fermi-LAT detections were $<3\sigma$ significance (Franckowiak et al. 2018).

2.2. γ-Ray Properties

Parameterizations of the γ-ray light curves for our 13 novae are provided in Table 1, taken from the references listed therein. Time$_{\gamma\text{-ray end}}$ and time$_{\gamma\text{-ray end}}$ denote the time range during which γ-rays are detected at $>2\sigma$ significance when binning Fermi-LAT light curves with a 1 day cadence. The γ-ray flux column lists the average flux over this time period, fitting a single power law to the data over the energy range of >100 MeV. Table 1 also lists the photon index for a single power-law fit to the Fermi-LAT data with energy >100 MeV:

$$\frac{dN}{dE} \propto E^{-\Gamma}, \tag{1}$$

where N is the number of photons, E is the photon energy, and Γ is the photon index. Although a single power law may not be the most physically motivated model, it is the simplest (most justified in cases of a low signal-to-noise ration (S/N)), and most widely quoted in studies of the various novae. It is sufficient for estimating γ-ray luminosities to the precision required for this study; modeling with a more complex exponentially cutoff power-law spectrum yields fluxes 75%–85% of that of a simple power law (Ackermann et al. 2014).

The γ-ray detections of novae V407 Lup and V357 Mus have been announced in Cheung et al. (2016a) and Li et al. (2018b), respectively, but a full analysis of their light curves has not yet been published. We therefore provide this analysis here in the following subsections.

2.2.1. Fermi-LAT Data Reduction

We downloaded the LAT data (Pass 8, Release 3, Version 2 with the instrument response functions of `P8R3_SOURCE_V2`) from the data server at the Fermi Science Support Center. For data reduction and analysis, we used `fermitools` (version 1.0.5) with `fermitools-data` (version 0.17)[7]. For data selection, we used a region of interest 14° on each side, centered on the nova. Events with the class `evclass=128` (i.e., SOURCE class) and the type `evtype=3` (i.e., reconstructed tracks FRONT and BACK) were selected. We excluded events with zenith angles larger than 90° to avoid contamination from the Earth's limb. The selected events also had to be taken during good time intervals, which fulfils the `gtmktime` filter `(DATA_QUAL>0)&&(LAT_CONFIG==1)`.

Next, we performed a binned likelihood analysis on the selected LAT data. For each nova, a γ-ray emission model for

[7] https://fermi.gsfc.nasa.gov/ssc/data/analysis/software/

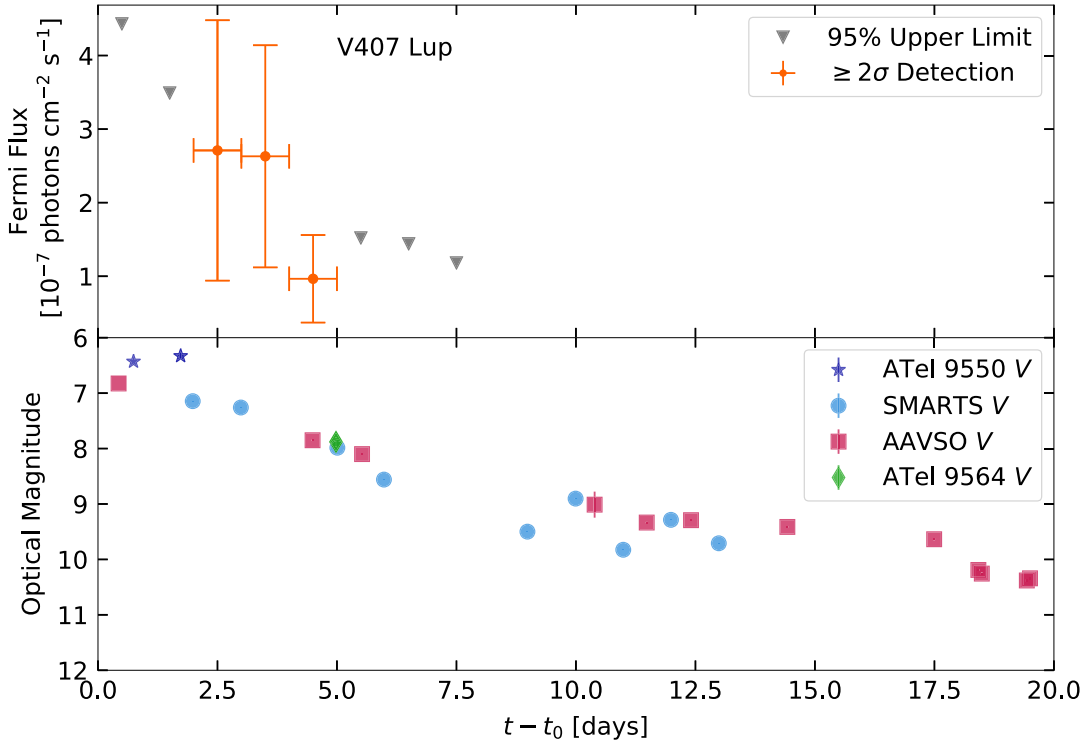

Figure 1. Top panel: the γ-ray light curve (>100 MeV) of V407 Lup. Bottom panel: the V-band optical light curve of V407 Lup. t_0 is taken to be the time of discovery, 2016 September 24.

Table 1
Characteristics of γ-Ray Detections of Novae (2010–2018), in Reverse Chronological Order

Nova	$\text{Time}_{\gamma\text{-ray start}}$ (MJD)	$\text{Time}_{\gamma\text{-ray end}}$ (MJD)	GeV γ-ray Flux (10^{-7} photon s^{-1} cm^{-2})	Photon index	Reference
V392 Per	58238[a]	58246	2.2 ± 0.4	2.0 ± 0.1	10,11
V906 Car	58216[b]	58239–58250[b]	12.2 ± 0.4	2.04 ± 0.02	9
V357 Mus	58129	58156	1.3 ± 0.2	2.2 ± 0.1	8, This work
V549 Vel	58037	58070	0.4 ± 0.2	1.8 ± 0.2	6,7
V5856 Sgr	57700	57715	4.6 ± 0.5	2.11 ± 0.05	5
V5855 Sgr	57686	57712	3.0 ± 0.8	2.26 ± 0.12	4
V407 Lup	57657	57660	1.6 ± 0.7	2.2 ± 0.3	3, This work
V5668 Sgr	57105	57158	1.1 ± 0.2	2.42 ± 0.13	2
V1369 Cen	56634	56672	2.5 ± 0.4	2.37 ± 0.09	2
V339 Del	56520	56547	2.3 ± 0.3	2.26 ± 0.08	1
V959 Mon	56097	56119	4.8 ± 0.6	2.34 ± 0.09	1
V1324 Sco	56093	56110	5.9 ± 0.9	2.16 ± 0.09	1
V407 Cyg	55265	55287	5.8 ± 0.6	2.11 ± 0.06	1

Notes.
[a] Due to Fermi-LAT downtime, data are not available for MJD 58224–58238. When observations resumed on MJD 58238, V392 Per was immediately detected. The γ-ray flux is calculated over MJD 58238–58246.
[b] Due to Fermi-LAT downtime, the start time of γ-ray detection for V906 Car was not captured, and the end time is only constrained to be within a date range. The γ-ray flux is calculated over MJD 58216–58239.
References. (1) Ackermann et al. (2014), (2) Cheung et al. (2016b), (3) Cheung et al. (2016a), (4) Nelson et al. (2019), (5) Li et al. (2017b), (6) Li et al. (2017a), (7) Li et al. (2020), (8) Li et al. (2018b), (9) Aydi et al. (2020b), (10) Li et al. (2018a), (11) B. Linnemann et al. (2020, in preparation).

the whole region of interest was built using all of the 4FGL cataloged sources located within 20° of the optical position (The Fermi-LAT collaboration 2020). As the two novae were the brightest γ-ray sources in the fields (within at least 5° according to the preliminary results), we only freed the normalization parameters for those cataloged sources located less than 1° from the targets. In addition, the Galactic diffuse emission and the extragalactic isotropic diffuse emission were included by using the Pass 8 background models `gll_iem_v07.fits` and `iso_P8R3_SOURCE_V2_v1.txt`, respectively, which were allowed to vary during the fitting process.

2.2.2. γ-Rays from V407 Lup

Nova V407 Lup (ASASSN-16kt) was discovered by the All-Sky Automated Survey for Supernovae (ASAS-SN) on 2016 September 24 UT at $V = 9.1$ (Stanek et al. 2016; Aydi et al. 2018b). The nova

was first detected in γ-rays on the same day as its optical discovery but did not reach a significance of $\geqslant 3\sigma$ until the next day, when the detection significance reached 4σ (with a test statistic, TS = 16.6). The average flux over the detection duration was $(1.6 \pm 0.7) \times 10^{-7}$ photon s^{-1} cm^{-2}. A single power-law fit gives a photon index of 2.2 ± 0.3.

The γ-ray light curve, shown in the top panel of Figure 1, shows a decrease in flux, completely fading below the LAT detection limit by 5 days after discovery. This makes V407 Lup's γ-ray duration the shortest known to date for a nova (Table 1). The bottom panel of Figure 1 shows the optical behavior of V407 Lup in the V band during and shortly after the γ-ray period. This light curve is constructed from publicly available photometry from the American Association of Variable Star Observers (AAVSO; Kafka 2020) and the Stony Brook/SMARTS Atlas (SMARTS photometry can be found at[8]; Walter et al. 2012), along with Chen et al. (2016) and Prieto (2016). The optical light curve rapidly declines alongside the γ-rays, exhibiting the shortest t_2 value of any nova in our sample (Table 2). The light curve shows what could possibly be a lag in the γ-ray emission compared to the optical. However, the date of the optical peak as estimated by Aydi et al. (2018a) is MJD 58656.4, implying that the first 3σ γ-ray detection lags the optical peak by only 0.6 day. Based on the cadence of the optical and γ-ray observations, which is around 0.5 day, this delay may be insignificant. A delay between the optical and γ-ray emission, if it exists, would have significant implications on our understanding of shock formation and γ-ray emission in novae (see e.g., Metzger et al. 2015 and Aydi et al. 2020b).

2.2.3. γ-Rays from V357 Mus

Nova V357 Mus was discovered in the optical on 2018 January 14.5 UT at ~7 mag (Kaufman et al. 2018). It was first detected in γ-rays 8 days later (Li et al. 2018b). The average >100 MeV flux over the detection period was $(1.3 \pm 0.2) \times 10^{-7}$ photon s^{-1} cm^{-2}, and the photon index from fitting a single power law was $\Gamma = 2.2 \pm 0.1$. The detection significance was 10σ over this period (with a TS = 98. 6).

The γ-ray light curve is shown in the top panel of Figure 2. There may be variability of a factor of ~2 in the light curve, but the low S/N makes it challenging to confidently measure this variability. The corresponding optical light curve is shown in the bottom panel of Figure 2, with data from ASAS-SN (Shappee et al. 2014), the Stony Brook/SMARTS Atlas, and AAVSO. The nova was detected by ASAS-SN on the rise to optical maximum but quickly became so bright that it saturated the detectors. Observations resumed around day 10 when amateur observers found the nova and began taking data (Kaufman et al. 2018). The nova likely reached a magnitude brighter than 6 mag at optical maximum (which was sometime between 0 and 10 days after the ASAS-SN pre-maximum detection). While the cadence and S/N of the γ-ray and optical light curves are not high enough to confirm, this nova may show evidence of correlated variation between the optical and γ-ray light curves, similar to the two brightest γ-ray novae V906 Car (Aydi et al. 2020b) and V5856 Sgr (Li et al. 2017b).

[8] http://www.astro.sunysb.edu/fwalter/SMARTS/NovaAtlas/

2.3. Optical Properties

Table 2 presents the main characteristics of the novae in our sample, some of which are compiled from the literature (with references given in parentheses following each table entry) and others estimated for the first time here. It includes the date of first detection in eruption (t_0) in MJD and UT, optical magnitude at t_0, peak magnitude in the V band ($V_{\rm max}$), and the time for the optical light curve to decline by two magnitudes from the maximum (t_2). The peak magnitude and t_2 are determined from reports in the literature or derived in this work using publicly available photometry from the AAVSO, ASAS-SN, and the Stony Brook/SMARTS Atlas. t_2 is measured as the duration between the first peak and the last time the nova reaches two magnitudes fainter than the peak.

We also list whether or not the nova formed dust based on reports in the literature or examining publicly available optical and near-infrared photometry, particularly from SMARTS and AAVSO, to search for dust dips in the optical light and/or IR excess. For some novae, we cannot tell if the nova has formed dust or not due to lack of multiband photometric follow-up.

We give the spectroscopic class (FeII or He/N; Williams 1992) and the FWHM of Balmer emission lines after optical peak. The spectroscopic classes are based on previous reports in the literature or determined based on spectra obtained around optical peak ($\lesssim t_2$). These spectra are either publicly available spectra from the Astronomical Ring for Access to Spectroscopy (ARAS[9]; Teyssier 2019) or from our private database. The FWHM are measured from the same spectra by fitting a single Gaussian profile to the Balmer emission lines. Nova V959 Mon is an exception since this nova was discovered in optical 56 days after its γ-ray detection by Fermi-LAT due to solar conjunction. The optical spectrum we use to determine the FWHM has been obtained 3 days after its optical discovery (around 60 days after the optical peak, given that for most novae the γ-ray detection occurs near the optical peak).

We also use high-resolution optical spectroscopy to estimate the Galactic column density toward each nova. Again, these spectra are either from ARAS or from our private database, and are obtained near the light-curve peak. We measure the equivalent widths of some diffuse interstellar bands and use the empirical relations of Friedman et al. (2011) to derive an estimate of $E(B-V)$. A_V is then derived assuming an extinction law of $R_V = 3.1$. This A_V is converted into an absorbing column density, $N(H)$, using the relation from Bahramian et al. (2015): $N(H) = (2.81 \pm 0.13) \times 10^{21} A_V$.

We also list distance estimates to the novae in our sample. For novae without an accurate distance estimate in the literature, we estimate the distance using our derived extinction values, along with the 3D Galactic reddening maps of Chen et al. (2019). We avoid using Gaia parallaxes to derive the distance for these novae because their parallaxes suffer from large uncertainties. Also, no nova in our sample belongs to the "Gold" or "Silver" samples of Schaefer (2018b), which have accurate Gaia distances.

In our nova sample, one system is known to have a Mira giant secondary, namely, V407 Cyg. The other 12 novae in the sample are likely systems with dwarf secondaries and will be designated as "classical novae" in the rest of the paper. However, it should be noted that V392 Per was recently found

[9] http://www.astrosurf.com/aras/Aras_DataBase/Novae.htm

Table 2
Nova Properties

Name	t_0[a] (MJD)	t_0[a] (Date, UT)	Discovery Mag[b] (mag)	V_{max} (mag)	Dust? (Y/N)	t_2 (days)	Spec. Class	FWHM (km s^{-1})	Distance (kpc)	N(H) (10^{21} cm^{-2})
V392 Per	58237.47 (1)	2018-04-29.47 (1)	∼6.2 (1)	5.6 (2)	⋯	3 (29)	Fe II (2)	4700±200 (2)	$4.1^{+2.3}_{-0.4}$ (25)	3.4 ± 0.4 (2)
V906 Car	58193.03 (28)	2018-03-16.03 (28)	<10[c] (3)	∼5.9 (28)	Y (28)	44 ± 2 (28)	Fe II (28)	1500 ± 100 (2)	4.0 ± 1.5 (28)	3.1 ± 0.4 (2)
V357 Mus	58121.24 (4)	2018-01-3.24 (4)	7.0 (5)	7.0 (5)	⋯	40±5 (2)	Fe II (5)	1200 ± 100 (2)	3.2 ± 0.5 (2)	4.2 ± 0.8 (2)
V549 Vel	58020.39 (6)	2017-09-24.39 (6)	∼11.3 (6)	9.1 (2)	⋯	90 (2)	Fe II (7)	2300 ± 200 (2)	>4 (2)	9.0 ± 1.0 (2)
V5856 Sgr	57686.02 (8)	2016-10-25.02 (8)	∼13.7 (9)	5.4 (8)	⋯	10 (8)	Fe II (8)	1600 ± 100 (2)	2.5 ± 0.5 (2)	3.1 ± 0.4 (2)
V5855 Sgr	57681.38 (11)	2016-10-20.84 (11)	10.7[d] (11)	7.5 (11)	⋯	17±2 (2)	Fe II (12)	200 ± 200 (2)	4.5 (11)	⋯
V407 Lup	57655.00 (13)	2016-09-24.00 (13)	∼9.1 (13)	<5.6 (14)	N (2)	3 ± 1 (5)	He/N (14)	2900 ± 100 (2)	4.2 ± 0.5 (2)	9.0 ± 1.2 (2)
V5668 Sgr	57096.63 (15)	2015-03-15.63 (15)	6.0[d] (15)	4.4 (16)	Y (17)	75 ± 2 (2)	Fe II (2)	1300 ± 100 (2)	2.8 ± 0.5 (2)	5.9 ± 0.8 (2)
V1369 Cen	56628.69 (18)	2013-12-2.69 (18)	5.5[d] (18)	∼3.3 (2)	Y (2)	40 ± 2 (2)	Fe II (2)	1200 ± 100 (2)	1.0 ± 0.4 (2)	0.6 ± 0.1 (2)
V339 Del	56518.58 (19)	2013-08-14.58 (19)	6.8[d] (19)	∼4.3 (2)	N (2)	11 ± 1 (2)	Fe II (2)	1700 ± 100 (2)	4.9 ± 1 (2)	1.7 ± 0.4 (2)
V959 Mon	56097.00 (20)	2012-06-19.00 (20)	∼9.9 (2)	N/A[f] (27)	N (2)	10 (2)	He/N (21)	2000 ± 200 (2)	1.4 ± 0.4 (26)	3.4 ± 0.4 (2)
V1324 Sco	56069.80 (22)	2012-05-22.80 (22)	18.5[e] (23)	9.8 (2)	Y (22)	24 (29)	Fe II (22)	1900 ± 200 (2)	>6.5 (29)	10.1 ± 0.7 (2)
V407 Cyg	55265.81 (24)	2010-03-10.81 (24)	6.8[d] (24)	7.1 (24)	⋯	5.9 (24)	He/N (24)	1400 ± 100 (2)	3.4 ± 0.5 (2)	5.6 ± 0.8 (2)

Notes.
[a] Date of first observation in eruption.
[b] *V* band, unless otherwise noted.
[c] Image was saturated.
[d] Image was obtained in an unfiltered optical band.
[e] Image was obtained in the *I* band.
[f] Optical maximum was during solar conjunction, so was missed.

References. (1) Munari & Ochner (2018), (2) This work, (3) Stanek et al. (2018), (4) ASAS-SN data Walter (2018), (5) Aydi et al. (2018a), (6) Stanek et al. (2017), (7) Luckas (2017), (8) Li et al. (2017b), (9) AAVSO Alert 561; (10) Munari et al. (2017), (11) Nelson et al. (2019), (12) Luckas (2016), (13) Stanek et al. (2016), (14) Aydi et al. (2018b), (15) Cheung et al. (2016b), (16) Gehrz et al. (2018), (17) Banerjee et al. (2015), (18) Waagen et al. (2013), (19) Waagen (2014), (20) Ackermann et al. (2014), (21) Munari (2013), (22) Finzell et al. (2018), (23) Wagner et al. (2012), (24) Munari et al. (2011), (25) Schaefer (2018a), (26) Linford et al. (2015), (27) Shugarov et al. (2014), (28) Aydi et al. (2020b), (29) Chochol et al. (2021), (30) Finzell et al. (2015).

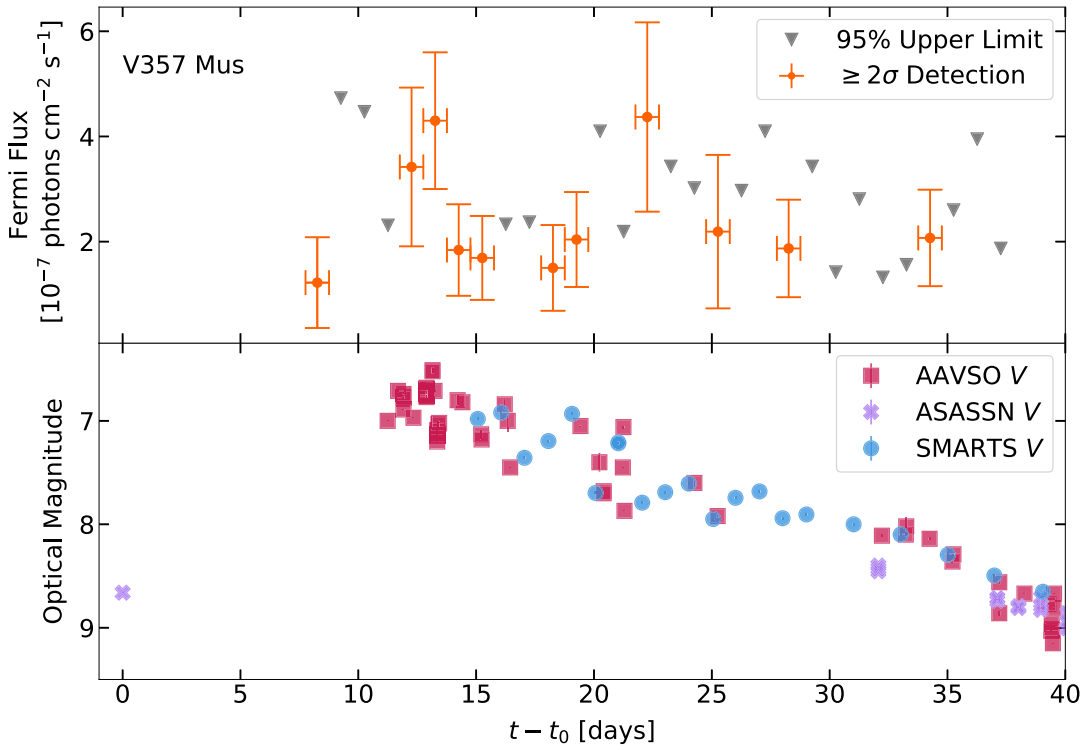

Figure 2. Top panel: the γ-ray light curve (>100 MeV) of V357 Mus. Bottom panel: the *V*-band optical light curve of V357 Mus. t_0 is taken to be the time of first observation in outburst, 2018 January 3.

to have a mildly evolved secondary star, with a binary orbital period of 3.4 days (Munari et al. 2020), implying that V392 Per may be a "bridge" object between embedded novae with dense circumstellar material and classical novae with low-density surroundings.

3. X-Ray Light Curves

3.1. Swift-XRT Observations

The Swift-XRT data products generator (Evans et al. 2007, 2009) was used to produce X-ray (0.3–10 keV) light curves for all the novae in our sample. The same tool was also used to divide the XRT flux into soft (0.3–1.0 keV) and hard (1–10 keV) X-ray bands. Once the data products were generated, the X-ray count rates were filtered to separate the significant detections from the upper limits. Observations with less than 3σ confidence on their count rates were considered upper limits. We quote 3σ upper limits throughout this paper, calculated using the uncertainty on the count rate.

In Figures A1–A13, we present the Swift X-ray (0.3–10 keV) light curves of all the novae in our sample. In each figure's top panel, we plot the total XRT count rate, while the bottom panel distinguishes the light curves in the soft and hard bands. The time range of the Fermi-LAT γ-ray detection is marked as a yellow bar, and the light curves focus on the first year following nova discovery.

There are Swift observations concurrent with Fermi-LAT γ-ray detections for nine of the 13 novae in our sample. Unfortunately, for some of the Fermi-detected novae, Swift observations were not obtained until long after discovery, and were therefore only detected after the end of the Fermi detection. Early observations were limited by solar conjunction for V392 Per, V959 Mon, and V549 Vel.

Many γ-ray detected novae are very optically bright, and lead to optical loading of the XRT if observed in photon counting mode.[10] Therefore, some Swift/XRT observations early in our targets' eruptions were obtained in the less sensitive windowed timing mode. This affects the observations of V906 Car, V357 Mus, V1369 Cen, V5668 Sgr, and V5856 Sgr. The supplementary online tables list information on each observation used, including the corresponding observation mode.

3.2. Hardness Ratio Evolution

We derive the hardness ratio (HR) for each Swift-XRT detection using the definition from Schwarz et al. (2011):

$$\mathrm{HR} = (H - S)/(H + S) \quad (2)$$

where S is the count rate in the 0.3–1.0 keV range and H is the count rate in the 1–10 keV range. We also use similar criteria as Schwarz et al. (2011) to classify the X-ray emission: we consider the X-ray emission "hard" if HR > -0.3, and "soft" if HR < -0.3.

In Figure 3 we present the evolution of the hardness ratio as a function of time since discovery for all the novae in our sample. The plot also shows the duration of the Fermi-LAT γ-ray detection, represented as a yellow box, to compare with the Swift X-ray observations. Non-detections, denoted as black tick marks in Figure 3, are defined as times when both the hard and soft bands were upper limits. If only one of the bands was detected, this epoch is counted as a detection, and the tick's color corresponds to the detected band.

The hardness ratio evolution of the novae is quite varied, but the main commonality is the lack of significant X-ray detection

[10] https://www.swift.ac.uk/analysis/xrt/optical_loading.php

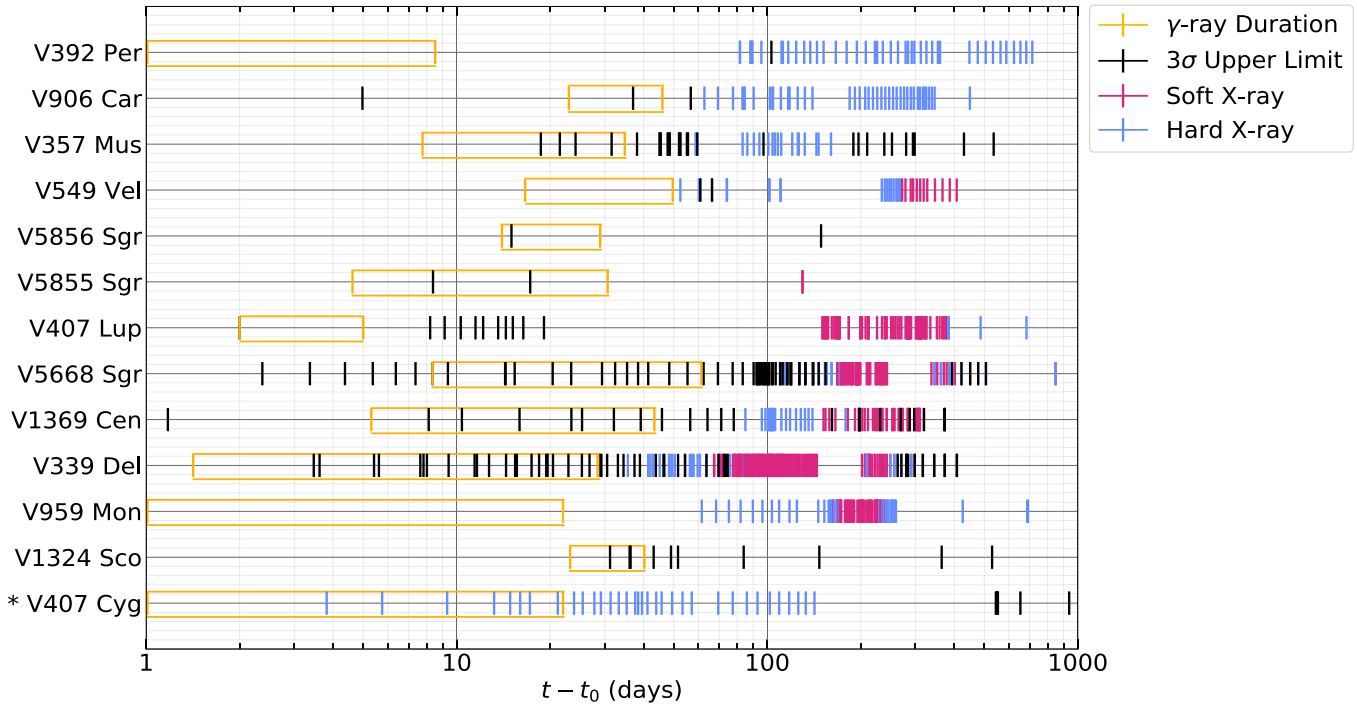

Figure 3. The evolution of the X-ray emission as a function of time since the discovery of our sample of Fermi-LAT-detected novae. Vertical tick marks represent the times of Swift-XRT observations, and are color coded according to the type of X-ray emission that was detected. Blue ticks denote hard X-ray emission, magenta ticks are soft X-ray emission, and black ticks represent X-ray non-detections. The durations of γ-ray detections with Fermi-LAT are denoted with yellow rectangles. V407 Cyg is marked with an asterisk to note that this system has a red giant secondary, unlike the other novae in our sample.

during the γ-ray emission period (with the exception of V407 Cyg).

4. Discussion

4.1. The Drivers of Hard X-Rays in Novae

Hard X-ray emission from optically thin plasma with a temperature of several KeV has long been observed in novae and is commonly attributed to shocks (e.g., O'Brien et al. 1994). Figure 4 compares the luminosity light curves in the 1–10 keV range for our nova sample. They have been smoothed to highlight bulk features; see Figures A1–A13 for full-cadence light curves. Distances are assumed as listed in Table 2. Count rates are corrected for foreground absorbing columns consistent with the intervening interstellar medium, using the $N(H)$ values quoted in Table 2. We do not account for intrinsic absorption (e.g., absorption from the nova ejecta). To make a rough conversion of the Swift-XRT count rate to X-ray flux, we assume a 5 keV thermal bremsstrahlung model (yielding the scale in units of erg s^{-1} on the right y-axis). The unabsorbed fluxes were then corrected for absorption using WebPIMMs as described above and then converted to luminosities scaled at a distance of 1 kpc.

This figure updates a similar plot from Mukai et al. (2008), with the goal of exploring the luminosities and durations of the hard X-ray emission from shocks. Figure 1 in Mukai et al. (2008) shows hard X-ray luminosity as a function of time for 16 novae, but most had very limited time coverage so the duration of hard X-rays was unclear. In our sample, we see that typically the hard X-rays become detectable 1–2 months after the start of eruption, and last several months to ~1 yr. The notable exception is V407 Cyg, whose hard X-rays evolve much faster, starting shortly after day 10 (concurrent with γ-ray detection). This rapid evolution may be attributable to interaction with circumbinary material around the secondary (Section 4.3); it is notable that other novae with giant companions, RS Oph (Bode et al. 2006; Sokoloski et al. 2006; Mukai et al. 2008), V745 Sco (Page et al. 2015), and V3890 Sgr Page et al. (2020b) were all detected in hard X-rays from the first pointed observations. However, RS Oph's last eruption occurred before the launch of Fermi, so we do not have information on its γ-ray evolution.

The 1–10 keV X-ray luminosities of novae in Figure 4 peak at 10^{33}–10^{34} erg s^{-1}. While we expect the bulk of the 1–10 keV luminosity to originate from shocked optically thin gas, in some cases it may be dominated by the hard tail of the supersoft component. For example, for moderate absorbing columns $N(H) \lesssim 10^{22}$ cm^{-2}, as expected for the Galactic foreground (Table 2), a $10^{37.5}$ erg s^{-1} blackbody of temperature $T_{\rm BB} = 90$ eV produces ~30 times as many counts in the 1–10 keV band[11] as a 10^{34} erg s^{-1} bremsstrahlung component with a temperature of 5 keV. Such a hot supersoft component is only expected for a near-Chandrasekhar mass white dwarf (e.g., Osborne et al. 2011), and contamination of the 1–10 keV band depends sensitively on the temperature of the supersoft source. A more typical white dwarf ($T_{\rm BB} \approx$ 60 eV; Wolf et al. 2013) of a similar luminosity contaminates the 1–10 keV band orders of magnitude less severely, contributing $\lesssim$30% of the 1–10 keV flux.

A detailed analysis of when the supersoft source contributes significantly to the 1–10 keV band would require spectral fitting of the Swift-XRT data and is outside the scope of this paper. However, in the case of a moderate absorbing column, the hardness ratio is a powerful discriminant. For

[11] https://heasarc.gsfc.nasa.gov/cgi-bin/Tools/w3pimms/w3pimms.pl

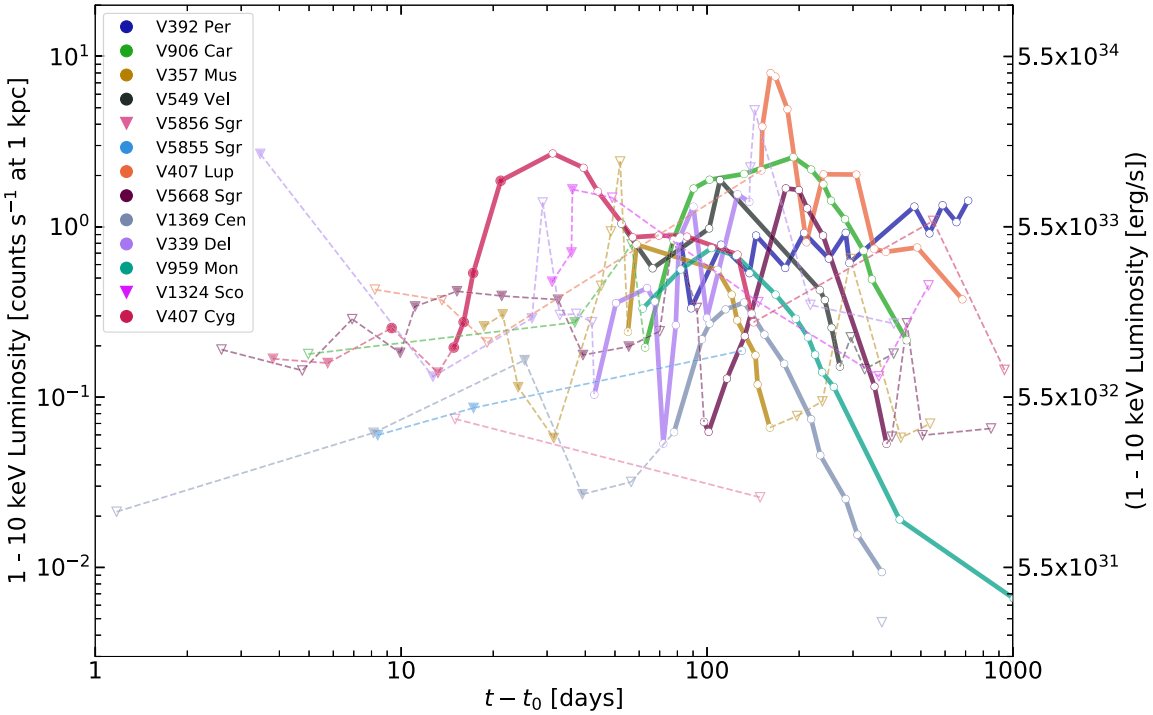

Figure 4. The luminosity in the hard X-ray band for all novae since the time the system was observed to be in eruption. When deriving these luminosities, we do not account for intrinsic absorption (e.g., absorption from the nova ejecta). Circles represent $\geqslant 3\sigma$ hard X-ray detections and triangles represent upper limits. Filled-in symbols denote concurrent hard X-ray and γ-ray emission, while open symbols were observed while γ-rays are not detected. Note that the light curves have been edited to better highlight trends.

$N(H) = 5 \times 10^{21}$ cm^{-2}, the count rate from a supersoft source should be $\gtrsim 10\times$ higher in the 0.3–1 keV band compared to the 1–10 keV band. For example, the 1–10 keV X-rays observed from V407 Lup starting around day 150 are likely the hard tail of the supersoft source because the concurrent 0.3–1 keV X-rays are so much brighter (Figure A7). At higher absorbing columns, the ratio of soft-to-hard X-rays from a supersoft source will be lower. In the case of V339 Del and V1369 Cen, some of the early 1–10 keV X-rays (day $\sim$50 and day $\sim$80, respectively) could be attributed to the supersoft source beginning to emerge from the absorbing nova ejecta, as the 0.3–1 keV flux is increasing during this time (Figures A9 and A10). However, in many of the novae studied here, the 1–10 keV flux is significantly brighter than the 0.3–1 keV flux and relatively stable in time (e.g., Figures A2, A3, A11), implying that the early hard X-rays really are emitted from hot shocked gas.

It is also possible that accretion could be a source of hard X-rays, particularly at late times. This is mainly true for systems with highly magnetized white dwarfs ($B > 10^6$ G), such as intermediate polars. In such systems, accretion is channeled by the strong magnetic field lines into an accretion column, which then slams onto the white dwarf surface at high speeds, increasing the surface temperature and leading to hard X-ray emission (see Warner 1995 for a review). Per, the hard X-ray emission in Nova V407 Lup around 350 days after eruption, is probably due to accretion resuming on the surface of the white dwarf (Figure A7). This nova occurred in an intermediate-polar system where the white dwarf is highly magnetized (see Aydi et al. 2018b for more details). The luminosity of hard X-ray emission in intermediate polars is usually $\sim 10^{31}$–10^{34} erg s^{-1} (Patterson 1994; Pretorius & Mukai 2014), which is consistent with the X-ray luminosity of V407 Lup around 2 yr after eruption.

Nova V392 Per also shows hard X-ray emission, which is peculiarly constant over a period of more than 250 days (see also F. J. Murphy-Glaysher et al. 2021, in preparation for a more detailed examination of the Swift data). As previously mentioned, this nova was recently found to have a mildly evolved secondary star (Munari et al. 2020). However, the origin of this constant and extended hard X-ray emission is not clear. While it could be accretion related, it is less likely to be due to shock interaction within the ejecta at this late stage. After the 1998 eruption of nova V2487 Oph, which is characterized by a $\sim$1 day orbital period (Anupama 2013), Hernanz & Sala (2002) found hard X-ray emission more than two years after the eruption with comparable luminosity to that of nova V392 Per ($\sim 10^{33}$ erg s^{-1}). Hernanz & Sala (2002) attributed this late X-ray emission to accretion resuming on the white dwarf. In addition, Orio et al.'s (2001) study of ROSAT observations of a large number of novae identified late X-ray emission from several novae during quiescence, which they attributed to accretion.

4.2. Novae with Dwarf Companions are Not Detected in 1–10 keV X-Rays Concurrent with γ-Rays

The internal shocks responsible for accelerating particles to relativistic speeds and producing γ-ray emission have velocities of $\sim$few thousand km s^{-1} and are expected to heat the post-shock gas to X-ray temperatures ($\sim 10^7$ K; Metzger et al. 2015). Therefore, it is surprising that we do not detect Swift X-ray emission concurrent with GeV γ-rays among the classical novae in our sample. Nine of the novae presented here have Swift-XRT observations during their Fermi-LAT detections, and all except V407 Cyg show no X-ray emission during this

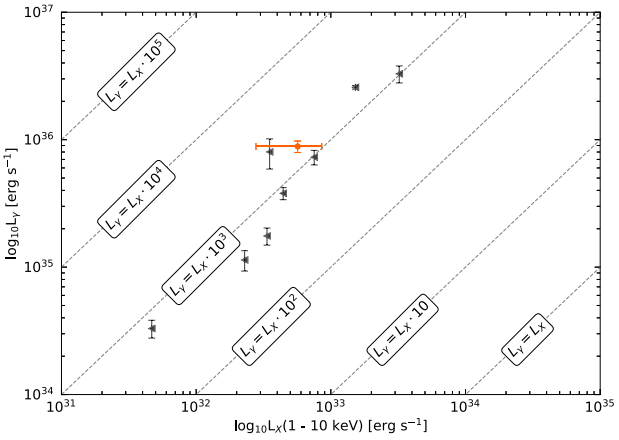

Figure 5. Comparison of hard X-ray and γ-ray luminosities for novae with concurrent X-ray and γ-ray data. X-ray luminosities are in the 1–10 keV band and corrected for Galactic absorption (as given in Table 2) and represent the faintest (and most constraining) X-ray points during the γ-ray detection period. Novae represented as black triangles denote that they are non-detections in the hard X-ray band, and 3σ upper limits are plotted. V407 Cyg is represented as an orange circle, as the only nova that had a $\geqslant 3\sigma$ Swift detection during the γ-ray detection period. γ-ray luminosities are calculated in the 100 MeV–300 GeV band using the parameters listed in Table 1. Dashed lines guide the eye for estimating L_γ/L_X.

period. The other four novae did not have Swift observations concurrent with Fermi-LAT detections. In all cases for the classical novae, the first X-ray detection only occurs after the γ-ray emission falls below the sensitivity limit of Fermi-LAT (Figure 3).

The simplest explanation for the Swift-XRT non-detections during γ-rays is that the shocks are deeply embedded within the nova ejecta due to their high density (among the highest for astrophysical transient events: $\sim 10^{10}$ cm^{-3}; see Figure 1 in Metzger et al. 2016). Such high densities imply substantial absorbing columns ahead of the shocks, which can absorb photons with energies $\lesssim$10 keV. The other explanation for the X-ray non-detections is that the thermal energy of the shocked material is sapped by cold regions around the shocks before it can be radiated, implying a suppression of the shock's temperature, i.e., the shocks do not reach X-ray energies (Steinberg & Metzger 2018). This would lead to a suppression of the X-ray emission that can be detected by Swift.

To constrain the conditions in nova shocks, we compare the Swift-XRT upper limits on the 1–10 keV X-ray luminosity with concurrent GeV γ-ray luminosities from Fermi-LAT (Figure 5). We convert the time-averaged Fermi-LAT γ-ray count rates listed in Table 1 to γ-ray fluxes assuming a single power-law spectrum and photon indices also listed in Table 1. The fluxes are then converted to luminosities over the energy range 100 MeV–300 GeV, assuming the distances in Table 2. The resulting γ-ray luminosities span a few $\times 10^{34}$ to a few $\times 10^{36}$ erg s^{-1}. The X-ray luminosities are as estimated for Figure 4 (Section 4.1). V392 Per, V549 Vel, V407 Lup, and V959 Mon are not plotted in Figure 5, as there were no X-ray observations during their γ-ray emitting periods. The γ-ray luminosities are factors at least 10^2–10^4 times more luminous than the X-ray upper limits, with most of the novae clustered around $L_\gamma/L_X \approx 10^3$. The ratios show a remarkable correlation, but no strong conclusions should be made as the plot is comparing a single data point in the X-rays per each nova to an averaged γ-ray luminosity over the detection period. The Swift upper limit depth is heavily dependent on exposure time and the background count rate.

Motivated by Swift non-detections, researchers have begun searching for even harder X-rays during the γ-ray bright phase using the NuSTAR satellite (Harrison et al. 2013), with instruments on board sensitive to photons with energies up to 79 keV. While softer X-rays are absorbed, harder X-rays >10 keV are expected to escape the dense ejecta, even in the early days of the eruption, due to the decreasing bound-free cross section at high photon energies (Metzger et al. 2015). Harder X-rays have now been detected with NuSTAR from three classical novae concurrently with γ-rays, namely, V5855 Sgr, V906 Car, and YZ Ret (YZ Ret is not included in our sample as it erupted in 2020; Nelson et al. 2019; Drake et al. 2020; Sokolovsky et al. 2020a, 2020b). Spectral analysis of these NuSTAR data show low-luminosity hard X-ray emission ($\sim 10^{33}$–10^{34} erg s^{-1}) originating from hot plasma ($kT \approx 5$–10 keV) and absorbed by large column densities ($N(H) \approx 10^{23}$–10^{24} cm^{-2}).

Even with these NuSTAR detections corrected for internal absorption, the L_γ/L_X ratio is still $\gtrsim 10 - 10^2$. The high L_γ/L_X observed with both Swift and NuSTAR is surprising because only a fraction of the shock's power should be going into producing γ-rays given the predicted efficiency for particle acceleration (Metzger et al. 2015). Meanwhile, the high post-shock densities imply that the shocks should be radiative, and so the majority of the shock luminosity should be promptly transferred to radiative luminosity, which is naively expected to emerge in the X-ray band (Metzger et al. 2015; Li et al. 2017b; Aydi et al. 2020b). Nelson et al. (2019) and Sokolovsky et al. (2020b) propose several scenarios that could yield a much higher γ-ray luminosity compared to X-rays, including separate shocks producing the X-rays and γ-rays, suppression of the X-rays by corrugated shock fronts (Steinberg & Metzger 2018), remarkably efficient particle acceleration, or that modeling the shocks as radiative is an improper assumption.

Of the 12 classical novae investigated here, 10 eventually show 1–10 keV hard X-ray emission detectable by Swift-XRT. This late emergence of the hard X-ray emission can be partially explained by a drop in the density of the ejecta as they expand —leading to a decrease in the absorbing column ahead of the shocks. But the faint NuSTAR detections imply that it is not only large absorbing columns that are leading to Swift non-detections; the X-ray luminosity is also intrinsically low.

4.3. The Exception: Novae with Giant Companions are Detected in X-Rays Concurrent with γ-Rays

Although evolved giant companions are relatively rare in nova-hosting binaries, the first-ever nova detected by Fermi-LAT, V407 Cyg, was accompanied by a Mira giant donor (Abdo et al. 2010). Previous to the nova eruption in 2010, V407 Cyg was well known as a D-type symbiotic star (e.g., Munari et al. 1990; Kolotilov et al. 1998, 2003). The giant donor's wind was dense, with a mass-loss rate of $\sim 10^{-6}$ $M_\odot$ yr^{-1}, resulting in a rich circumbinary medium (Chomiuk et al. 2012).

During its 2010 nova eruption (discovered on 2010 March 10), V407 Cyg displayed faint but detectable X-rays in the first Swift-XRT observations of the nova eruption (4 days after nova discovery; Figure A13, Shore et al. 2011; Nelson et al. 2012). Over the next ~20 days following the nova discovery, the X-ray flux rapidly brightened by a factor of ~10. During this same time period, V407 Cyg was detected as a GeV γ-ray source by Fermi-LAT (Abdo et al. 2010). V407 Cyg is the only nova in our sample with concurrent Swift-XRT and Fermi-LAT detections.

Both the X-rays and the γ-rays in V407 Cyg are attributed to the interaction of the nova ejecta with the circumbinary medium (Orlando & Drake 2012; Martin & Dubus 2013). The X-ray flux rises in the first 3 weeks because the absorbing column might have dropped, while the X-ray emission measure grows. The absorbing column, even at early times, is never much higher than $N(H) \approx 10^{23}$ cm^{-2} (Nelson et al. 2012). This can be contrasted with the absorbing columns of $\gtrsim$ few $\times 10^{23}$ cm^{-2} for the internal shocks observed in classical novae with dwarf companions (e.g., Nelson et al. 2019; Sokolovsky et al. 2020b). Therefore, V407 Cyg hints that X-rays can be detected concurrently with γ-rays if the nova drives *external* shocks (i.e., interaction with preexisting circumbinary material), as opposed to more deeply absorbed shocks internal to the nova ejecta.

This hypothesis is supported by two additional novae with giant companions that were marginally detected by Fermi-LAT between 2010 and 2018: V745 Sco and V1535 Sco (Franckowiak et al. 2018). Hints of γ-ray emission from V745 Sco were obtained at 2–3σ significance in the first 2 days of its 2014 nova eruption (Cheung et al. 2014). Bright hard X-ray emission was also observed during this time, with $N(H) =$ few $\times 10^{22}$ cm^{-2} (Delgado & Hernanz 2019; again, substantially lower than the absorbing columns observed for shocks in classical novae). Similarly, V1535 Sco was marginally detected in γ-rays during the first 7 days of its 2015 eruption (Franckowiak et al. 2018), and hard X-rays were concurrently detected by Swift-XRT (on day 4; Linford et al. 2017). Although these γ-ray detections are marginal, they support a scenario where nova shocks with external circumbinary material (as occur in binaries with giant companions) are characterized by lower density, less embedded environments, in comparison with shocks that occur internal to nova ejecta in binaries with dwarf companions.

In addition to the external shocks, would any internal shocks be present and contribute to the emission in novae with giant companions? One might argue that internal shocks are completely absent in novae with giant companions, for reasons related to the properties of the binary system and internal shocks formation scenario: internal shocks in novae with dwarf companions are likely formed by the interaction between two discrete ejections—a slow early ejection, possibly shaped by the binary motion in a common envelope phase, followed by a faster wind (Chomiuk et al. 2014; Das et al. 2015; Li et al. 2017b; Aydi et al. 2020b, 2020a). Given the large separations and orbital periods of novae with giant companions (the orbital period of V407 Cyg is at least 100 times longer than the next longest period system, V392 Per at 3.4118 days, in our sample), it could imply that common envelope ejection is not playing a role in these eruptions and therefore the mechanism of internal shocks formation in novae with dwarf companions does not apply here. One might also argue that even if internal shocks are present in novae with giant companions, the ejecta masses in these novae are so low that internal shocks contribution might be negligible compared to that of the external shocks.

It is worth noting that the high L_γ/L_X observed in V407 Cyg (see Figure 5) could not be explained by high absorption or X-ray suppression in this case, given the less embedded environments of the shocks. However, a detailed analysis of the shocks in novae with evolved secondaries is outside the scope of this paper and will be the topic of future projects.

4.4. Why are Some γ-Ray Detected Novae Never Detected in X-Rays?

Out of the 13 novae in our sample, only two were never detected as X-ray sources with Swift, namely, V1324 Sco (Figure A12; Finzell et al. 2018) and V5856 Sgr[12] (Figure A5; Li et al. 2017b). V5856 Sgr had only two Swift observations (15 and 149 days after discovery), which makes it difficult to draw conclusions about this nova as its X-ray emission could have been missed (as we might have missed the X-ray emission from, e.g., V357 Mus if observations of it had been similarly sparse). However, V1324 Sco was followed with Swift between days 30 and ~500 after eruption and was still never detected.

There are a few reasons that might explain why V1324 Sco was not detected: lack of correlation between γ-ray luminosity and X-ray luminosity, distance, and/or absorption. While V1324 Sco was not detected in X-rays, it is among the brightest novae detected in γ-rays. If X-ray luminosity does not scale with γ-ray luminosity, this could explain the difference between the two.

Distance, however, appears to be an important factor in the detection of X-rays. V1324 Sco is the farthest nova of our sample ($\gtrsim$6.5 kpc), and Figure 4 shows that this translates to less sensitive upper limits on the hard X-ray luminosity. We compared the flux of each nova's first 1–10 keV detection to what it would be at V1324 Sco's distance (also correcting for the additional interstellar absorption). This analysis revealed that five novae would have been non-detections at the distance and $N(H)$ of V1324 Sco: V906 Car, V357 Mus, V5856 Sgr, V5855 Sgr, and V5668 Sgr. We therefore conclude that distance is probably the reason why V1324 Sco was not detected by Swift-XRT.

4.5. What Determines When the Hard X-Rays Appear?

Part of the intention of this project was to study a sample of γ-ray detected novae in order to analyze possible trends in the data. In Figure 6, we plot the date of the first hard X-ray detection against other nova properties described in Sections 2.2 and 2.3: t_2, FWHM of Balmer emission lines (after optical peak), apparent magnitude at optical peak ($V_{\rm max}$), and the duration of the γ-ray detection to check for any correlations between these parameters. The Pearson correlation coefficient is shown in the top right corner of each panel.

Since the timings of Swift observations are different for each nova, it is challenging to draw conclusions about correlations between these parameters. For novae with extremely bright supersoft emission, it is possible that the harder shock component is contaminated by the supersoft component (see Section 4.1 for further discussion). The cadence for novae V407 Lup, V392 Per, and V5855 Sgr was interrupted by solar conjunction and observation schedules. In addition, V407 Lup and V5855 Sgr were first detected during a bright supersoft phase, which caused large uncertainties on the first hard X-ray start date for these novae, as plotted in Figure 6. Because of these complications, we exclude these novae from the fitting done to derive the correlation coefficients.

[12] After further analysis of the WT data of V5856 Sgr, there is a possible X-ray detection on day 149, but the online generator did not find any detection. This is mainly affected by the estimate of background contribution for faint objects observed in WT mode.

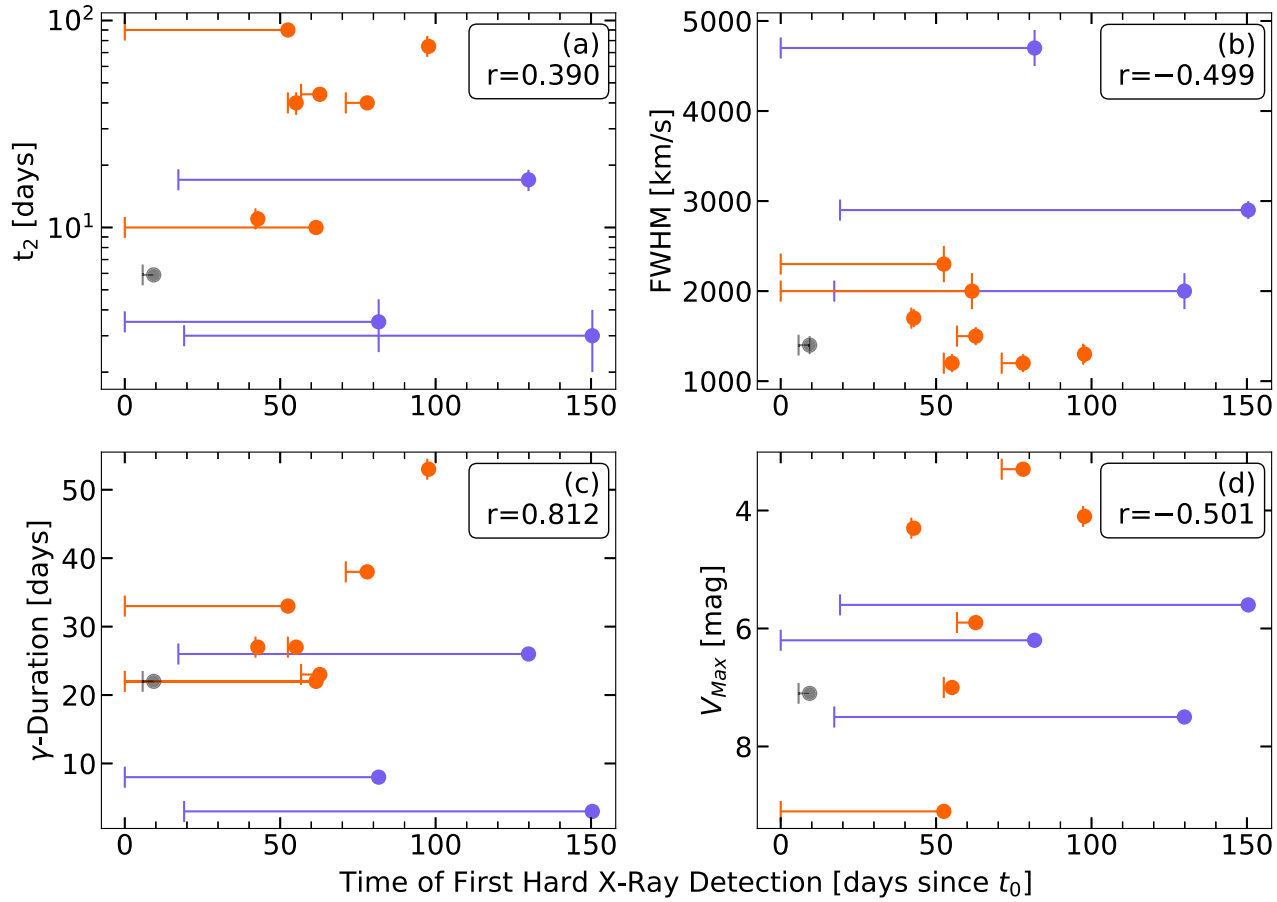

Figure 6. The date of the first hard X-ray detection since t_0 for each nova plotted against t_2 (panel (a)), FWHM (measured from the Balmer lines a few days after optical maximum; panel (b)), duration of detectable γ-rays (panel (c)), and apparent magnitude at optical peak (V_{max}; panel (d)) for the novae in our sample for which a measurement is available. The error in the first hard X-ray detection represents a lower limit on this quantity, extending to the date of the last non-detection; if the arrows extend to $t = t_0$, the first Swift-XRT observation was a 3σ detection. V407 Cyg is represented in dark gray in each panel as it has a giant companion (Section 4.3). The r value denoted in the upper right corner of each panel is the Pearson correlation coefficient derived by using the gray and orange circles in each panel and excluding any weight for the error bars. V392 Per, V407 Lup, and V5855 Sgr are plotted in purple as the actual hard X-ray start for these novae is uncertain (see Section 4.5 for more details); therefore, we exclude them from the correlation fitting. V1324 Sco and V5856 Sgr were never detected in X-rays by Swift (see Section 4.4) so they do not appear in the plots; V959 Mon does not appear in panel (d) as a maximum V-band magnitude could not.

Based on panel (a) in Figure 6, visual inspection indicates earlier hard X-ray emission for faster novae (characterized by smaller t_2)—particularly for novae with extensive Swift follow-up (with short error bars in Figure 6). The Pearson coefficient factor of $r = 0.39$ derived for novae with higher-quality data also implies that there may be a weak correlation. Interestingly, we find a weak anticorrelation between the time of first hard X-ray detection and FWHM ($r = -0.50$ shown in panel (b)). A nova characterized by a faster optical light curve (short t_2) should typically have higher ejecta expansion velocities (large FWHM; Shafter et al. 2011). In this case, the ejecta are expected to expand, drop in density, and become optically thin to the X-ray emitting shocked regions more rapidly than slower novae. There are hints in Figure 6 that we may be observing these trends, but a larger sample of novae will need to be observed in the future in order to confirm these hints.

In panel (c), a Pearson correlation coefficient of 0.81 implies a likely correlation between the duration of the γ-ray detection and the first hard X-ray detection. To first order, this is expected given that none of the novae in our sample recorded Swift X-ray detections concurrent with the γ-ray emission and were only detected after this period ended. But this correlation may hold important clues as to the drivers of shocks in novae, as the only other quantity that has been observed to potentially correlate with γ-ray duration is γ-ray fluence (Cheung et al. 2016b; Franckowiak et al. 2018).

Panel (d) shows some indication of a correlation between the peak brightness of the nova and the time of first hard X-ray detection (note that an anticorrelation here is a correlation with brightness, due to the "flipped" magnitude scale). However, again this correlation is weak and requires a larger sample or higher cadence data to test.

In summary, although there are intriguing hints at correlations, it is challenging to draw conclusions from the current sample—the number of novae detected in γ-rays with dedicated multiwavelength follow-up is still small. Additional novae with high-cadence Swift-XRT and optical follow-up added to the current sample will allow us to draw better conclusions in the future.

5. Summary and Conclusions

We have investigated the hard (1–10 keV) X-ray emission of 13 γ-ray emitting novae using Swift-XRT. Novae have long been

observed to emit X-rays from hot ($kT \approx 1$–10 keV) optically thin plasma, presumably from shocked gas (O'Brien et al. 1994; Mukai et al. 2008). The Swift-XRT light curves show evidence of hard X-ray emission from shocks in at least seven out of the 13 novae studied, typically peaking several months after the start of eruption with luminosities $\sim 10^{33}$–10^{34} erg s^{-1}.

However, of the nine novae with Swift-XRT observations during the γ-ray detection phase (typically a few weeks around optical maximum), eight yielded X-ray non-detections during these early times. The only nova showing X-ray emission concurrently with a Fermi γ-ray detection is V407 Cyg, which has a giant secondary. We suggest that the non-detection of early X-ray emission from the other eight novae (all with dwarf companions) is due to a combination of large column densities ahead of the shocks absorbing the X-rays and X-ray suppression by corrugated shock fronts (e.g., Metzger et al. 2015; Steinberg & Metzger 2018). The early X-ray detection of V407 Cyg (and possibly other novae with evolved companions) confirms that the shocks in symbiotic systems are external (between the nova ejecta and circumbinary material), rather than internal to the nova ejecta as claimed for novae with dwarf companions.

As more γ-ray emitting novae are discovered and followed up at other wavelengths, we will be able to better constrain the physical parameters of the shocks and further investigate the conditions of their surrounding media.

We are grateful to Tommy Nelson and Brian Metzger for conversations that inspired this work. A.C.G., E.A., L.C., K.V. S., and J.S. are grateful for the support of NASA Fermi grant 80NSSC18K1746, NuSTAR grant 80NSSC19K0522, NSF award AST-1751874, and a Cottrell Scholarship of the Research Corporation. K.L.P. acknowledges funding from the UK Space Agency. K.L.L. is supported by the Ministry of Science and Technology of the Republic of China (Taiwan) through grants 108-2112-M-007-025-MY3 and 109-2636-M-006-017, and he is a Yushan (Young) Scholar of the Ministry of Education of the Republic of China (Taiwan).

This work made use of data supplied by the UK Swift Science Data Centre at the University of Leicester. We acknowledge with thanks the variable star observations from the AAVSO International Database contributed by observers worldwide and used in this research. We also acknowledge with thanks the ARAS observers for their optical spectroscopic observations. We acknowledge with thanks the referee for the valuable comments.

Appendix
Swift X-Ray Light Curves

In this Appendix, we present the XRT X-ray (0.3–10 keV) light curves for all the novae in our sample in Figures A1–A13. We also plot the soft (0.3–1.0 keV) and hard (1.0–10 keV) light curves.

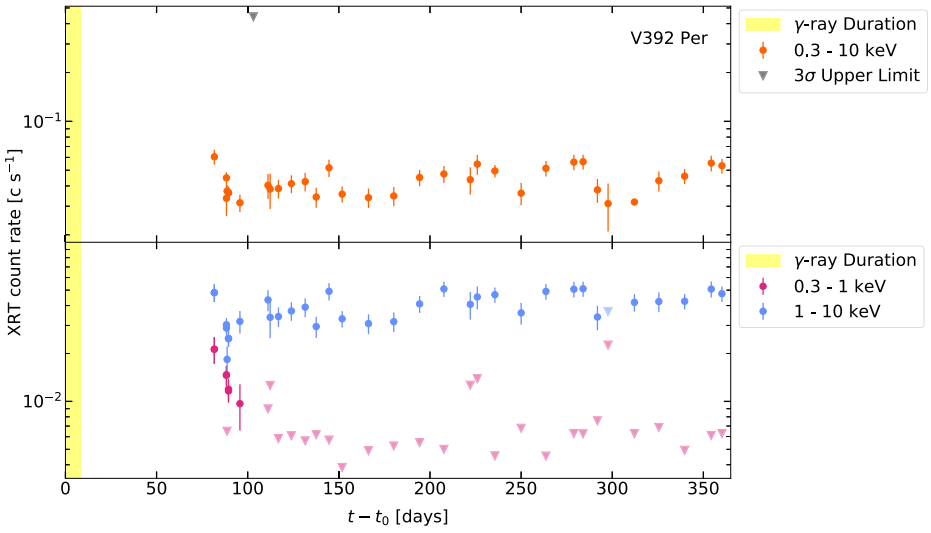

Figure A1. Swift-XRT X-ray light curves of V392 Per, plotted as a function of days since discovery ($t - t_0$). The upper panel plots the count rate over the full 0.3–10 keV energy range, with orange points representing detections and dark gray triangles representing 3σ upper limits. The lower panel splits the counts into hard (1.0–10 keV) and soft (0.3–1.0 keV) X-ray bands. The soft band is plotted in magenta, and the hard band is plotted in blue; in both cases, circles represent detections and triangles represent 3σ upper limits. The time range wherein Fermi-LAT detected γ-rays with $>3\sigma$ significances is marked as a yellow bar. Any purple points come from the hard and soft points overlapping each other. Similarly, darker colored full-band upper limits come from overlapping points. The data behind this figure is available in machine readable format.

(The data used to create this figure are available.)

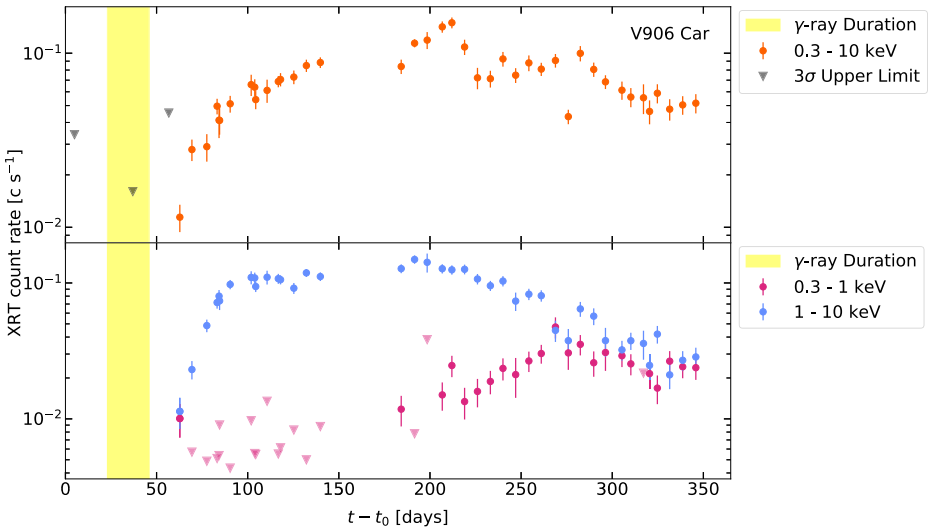

Figure A2. Swift-XRT X-ray light curves of V906 Car (ASASSN-18fv). See Figure A1 for more details. The data behind this figure is available in machine readable format.

(The data used to create this figure are available.)

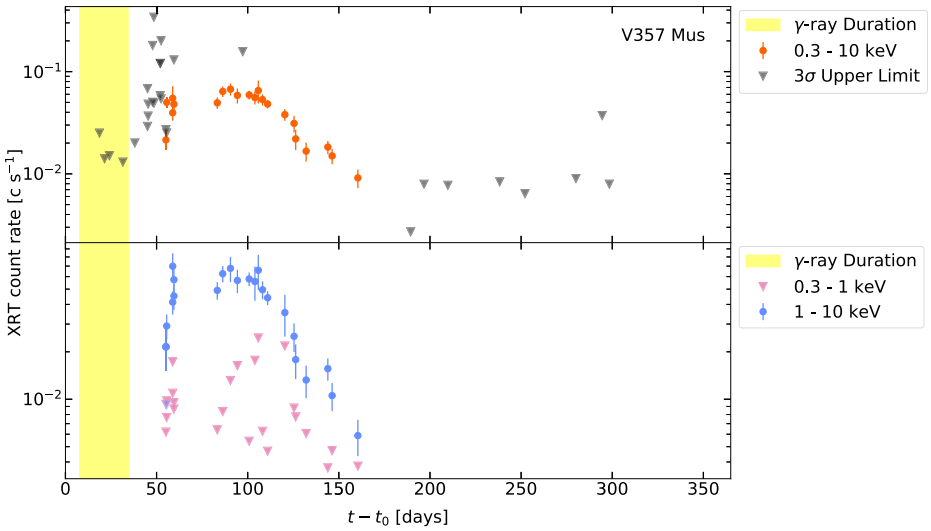

Figure A3. Swift-XRT X-ray light curves of V357 Mus. See Figure A1 for more details. The data behind this figure is available in machine readable format.

(The data used to create this figure are available.)

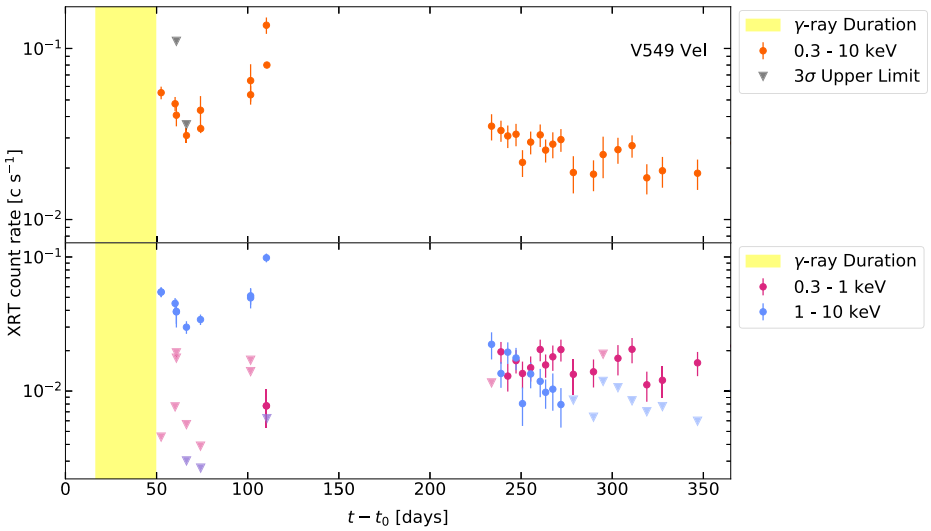

Figure A4. Swift-XRT X-ray light curves of V549 Vel (ASASSN-17mt). See Figure A1 for more details. The data behind this figure is available in machine readable format.

(The data used to create this figure are available.)

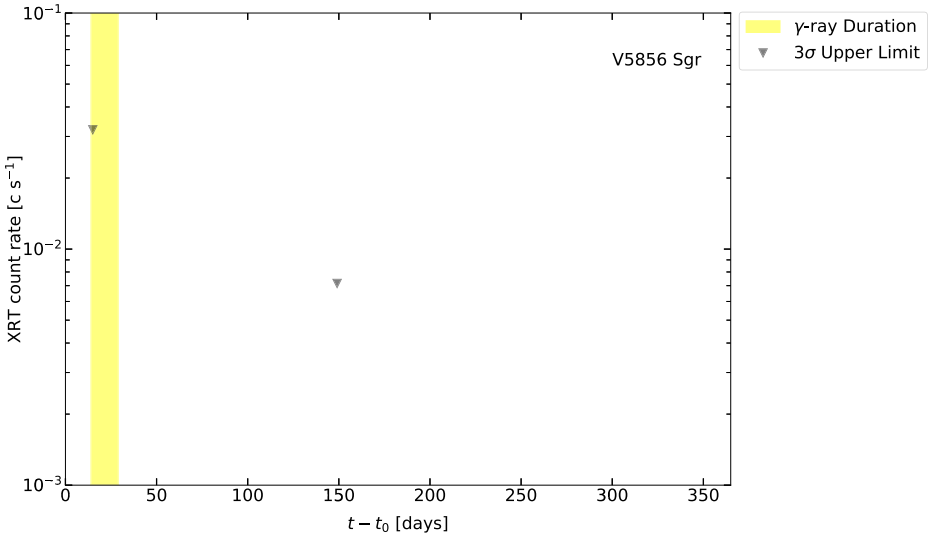

Figure A5. Swift-XRT X-ray light curve of V5856 Sgr (ASASSN-16ma). See Figure A1 for more details. The data behind this figure is available in machine readable format.

(The data used to create this figure are available.)

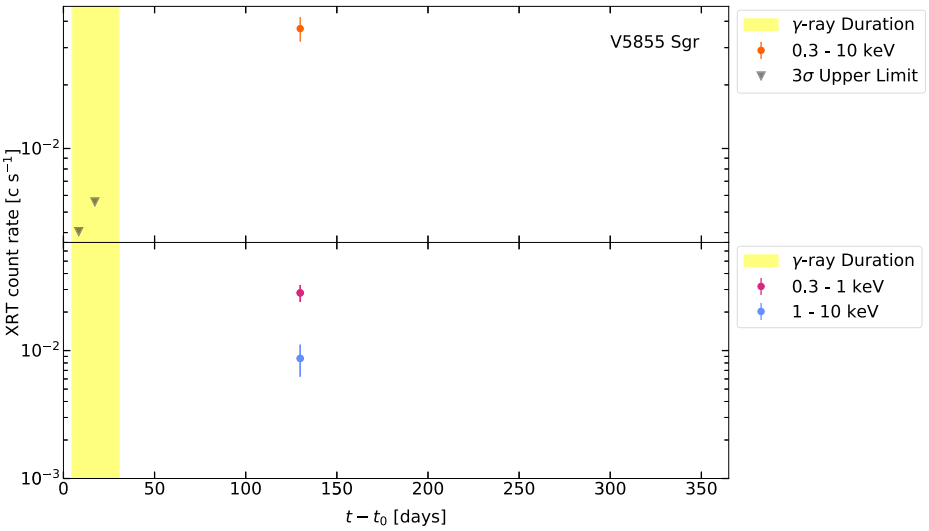

Figure A6. Swift-XRT X-ray light curves of V5855 Sgr. See Figure A1 for more details. The data behind this figure is available in machine readable format.
(The data used to create this figure are available.)

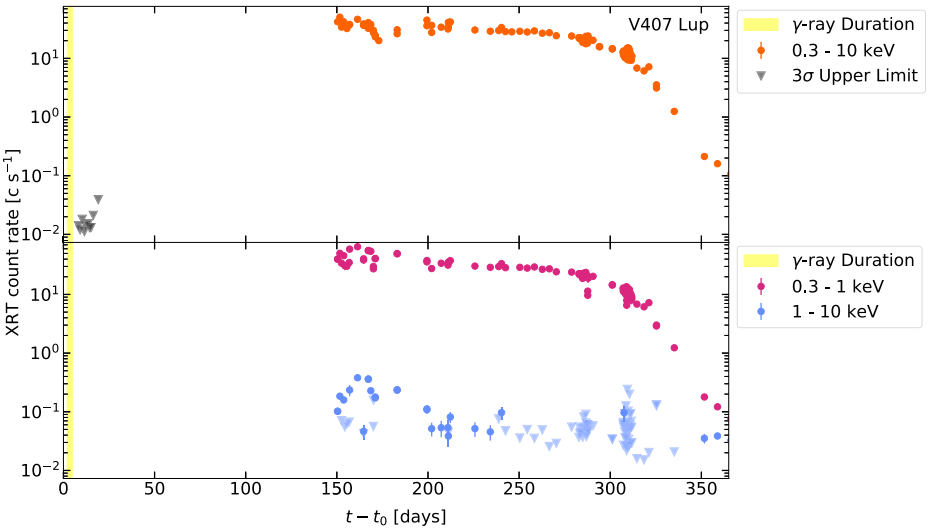

Figure A7. Swift-XRT X-ray light curves of V407 Lup (ASASSN-16kt). See Figure A1 for more details. The data behind this figure is available in machine readable format.
(The data used to create this figure are available.)

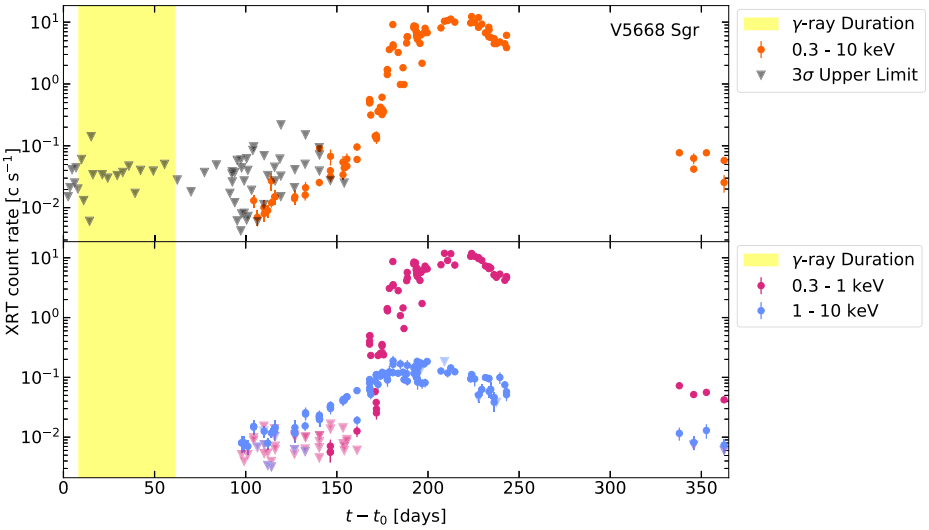

Figure A8. Swift-XRT X-ray light curves of V5668 Sgr. See Figure A1 for more details. The data behind this figure is available in machine readable format. (The data used to create this figure are available.)

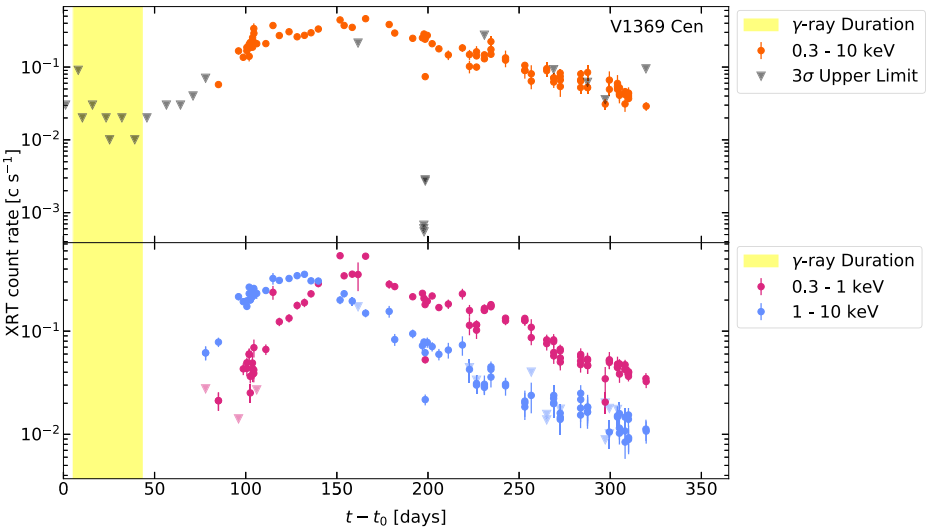

Figure A9. Swift-XRT X-ray light curves of V1369 Cen. See Figure A1 for more details. The data behind this figure is available in machine readable format. (The data used to create this figure are available.)

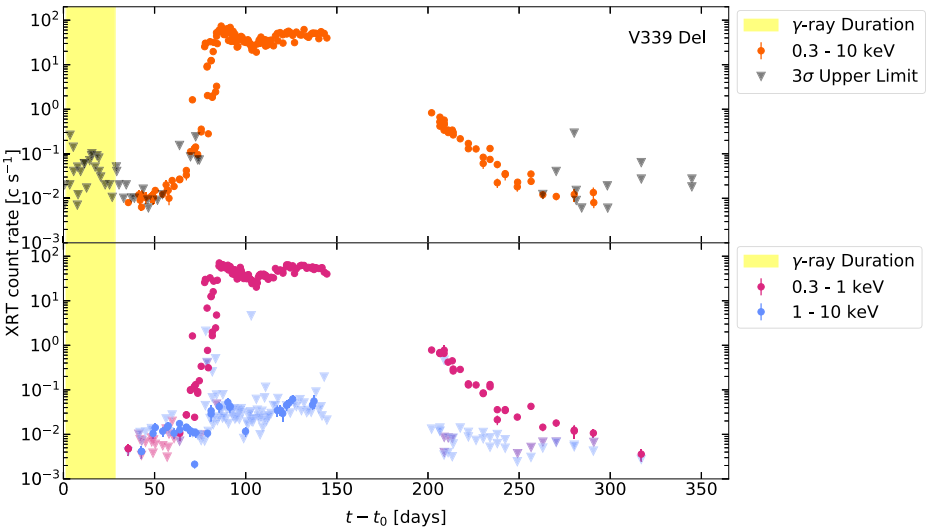

Figure A10. Swift-XRT X-ray light curves of V339 Del. See Figure A1 for more details. The data behind this figure is available in machine readable format. (The data used to create this figure are available.)

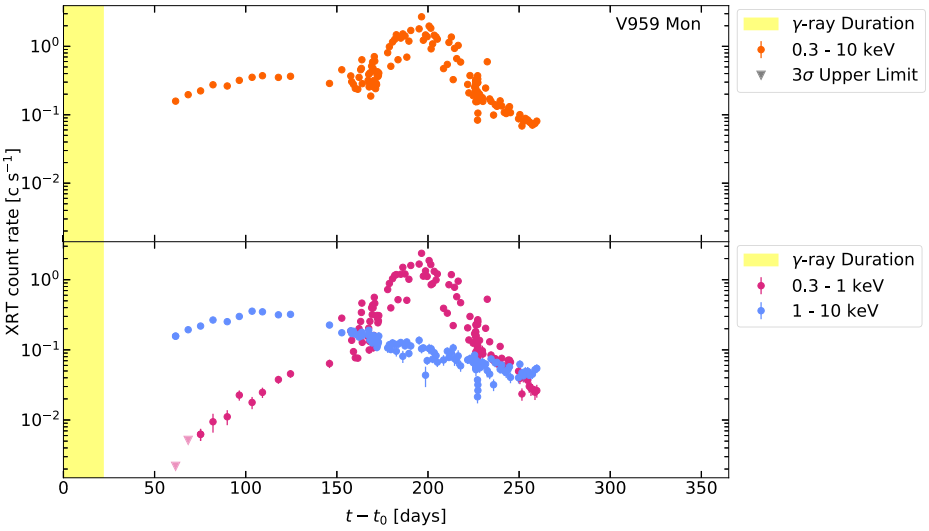

Figure A11. Swift-XRT X-ray light curves of V959 Mon. See Figure A1 for more details. The data behind this figure is available in machine readable format. (The data used to create this figure are available.)

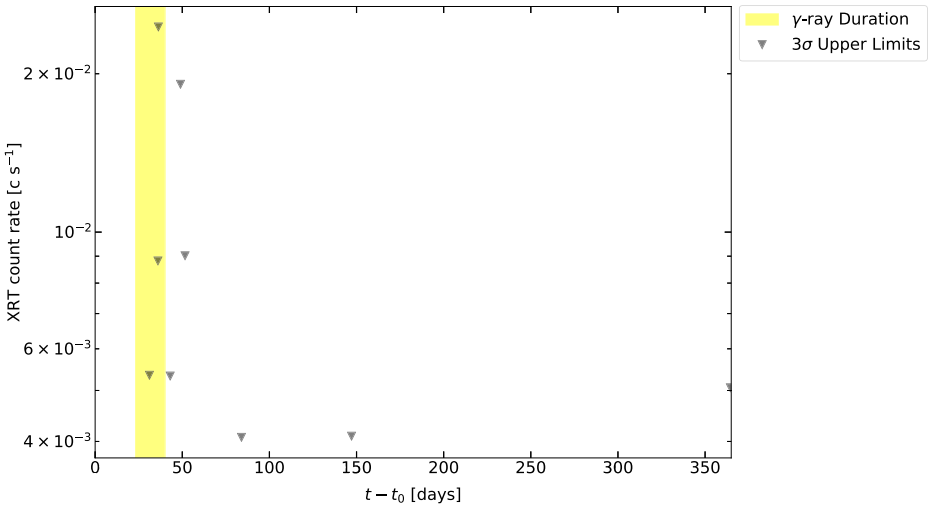

Figure A12. Swift-XRT X-ray light curve of V1324 Sco. See Figure A1 for more details. The data behind this figure is available in machine readable format. (The data used to create this figure are available.)

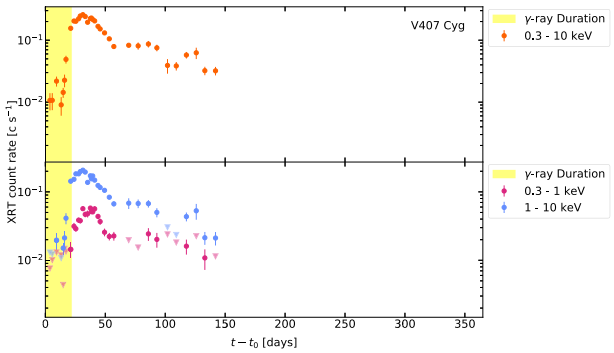

Figure A13. Swift-XRT X-ray light curves of V407 Cyg. See Figure A1 for more details. The data behind this figure is available in machine readable format.

(The data used to create this figure are available.)

ORCID iDs

A. C. Gordon https://orcid.org/0000-0002-5025-4645
E. Aydi https://orcid.org/0000-0001-8525-3442
K. L. Page https://orcid.org/0000-0001-5624-2613
Kwan-Lok Li https://orcid.org/0000-0001-8229-2024
L. Chomiuk https://orcid.org/0000-0002-8400-3705
K. V. Sokolovsky https://orcid.org/0000-0001-5991-6863
K. Mukai https://orcid.org/0000-0002-8286-8094

References

Abdo, A. A., Ackermann, M., Ajello, M., et al. 2010, Sci, 329, 817
Ackermann, M., Ajello, M., Albert, A., et al. 2014, Sci, 345, 554
Anupama, G. C. 2013, in IAU Symp. 281, Binary Paths to Type Ia Supernovae Explosions, ed. R. Di Stefano, M. Orio, & M. Moe (Cambridge: Cambridge Univ. Press), 154
Aydi, E., Buckley, D. A. H., Mohamed, S., & Whitelock, P. A. 2018a, ATel, 11221, 1
Aydi, E., Chomiuk, L., Izzo, L., et al. 2020a, ApJ, 905, 62
Aydi, E., Orio, M., Beardmore, A. P., et al. 2018b, MNRAS, 480, 572
Aydi, E., Sokolovsky, K. V., Chomiuk, L., et al. 2020b, NatAs, 4, 776
Bahramian, A., Heinke, C. O., Degenaar, N., et al. 2015, MNRAS, 452, 3475
Banerjee, D. P. K., Ashok, N. M., & Srivastava, M. 2015, ATel, 7748, 1
Bode, M. F., & Evans, A. 2008, Classical Novae, Vol. 43 (Cambridge: Cambridge Univ. Press)
Bode, M. F., O'Brien, T. J., Osborne, J. P., et al. 2006, ApJ, 652, 629
Burrows, D. N., Hill, J. E., Nousek, J. A., et al. 2005, SSRv, 120, 165
Chen, B.-Q., Huang, Y., Yuan, H.-B., et al. 2019, MNRAS, 483, 4277
Chen, P., Dong, S., Bose, S., et al. 2016, ATel, 9550, 1
Cheung, C. C., Jean, P., & Shore, S. N. 2014, ATel, 5879, 1
Cheung, C. C., Jean, P., Shore, S. N. & Fermi Large Area Telescope Collaboration 2016a, ATel, 9594, 1
Cheung, C. C., Jean, P., Shore, S. N., et al. 2016b, ApJ, 826, 142
Chochol, D., Shugarov, S., Hambálek, Ľ., et al. 2021, The Golden Age of Cataclysmic Variables and Related Objects (Palermo: POS)
Chomiuk, L., Krauss, M. I., Rupen, M. P., et al. 2012, ApJ, 761, 173
Chomiuk, L., Linford, J. D., Yang, J., et al. 2014, Natur, 514, 339
Das, R., Banerjee, D. P. K., Nandi, A., Ashok, N. M., & Mondal, S. 2015, MNRAS, 447, 806
Delgado, L., & Hernanz, M. 2019, MNRAS, 490, 3691
Drake, J. J., Orio, M., Bearmore, A., et al. 2020, ATel, 14214, 1
Evans, P. A., Beardmore, A. P., Page, K. L., et al. 2007, A&A, 469, 379
Evans, P. A., Beardmore, A. P., Page, K. L., et al. 2009, MNRAS, 397, 1177
Finzell, T., Chomiuk, L., Metzger, B. D., et al. 2018, ApJ, 852, 108
Finzell, T., Chomiuk, L., Munari, U., & Walter, F. M. 2015, ApJ, 809, 160
Franckowiak, A., Jean, P., Wood, M., Cheung, C. C., & Buson, S. 2018, A&A, 609, A120
Friedman, S. D., York, D. G., McCall, B. J., et al. 2011, ApJ, 727, 33
Gallagher, J. S., & Starrfield, S. 1978, ARA&A, 16, 171
Gallagher, J. S. I., & Code, A. D. 1974, ApJ, 189, 303
Gehrels, N., Chincarini, G., Giommi, P., et al. 2004, ApJ, 611, 1005
Gehrz, R. D., Evans, A., Woodward, C. E., et al. 2018, ApJ, 858, 78
Harrison, F. A., Craig, W. W., Christensen, F. E., et al. 2013, ApJ, 770, 103
Hernanz, M., & Sala, G. 2002, Sci, 298, 393
Kafka, S. 2020, Observations from the AAVSO International Database, https://www.aavso.org
Kaufman, R., Guido, E., Noschese, A., et al. 2018, CBET, 4473, 1
Kolotilov, E. A., Munari, U., Popova, A. A., et al. 1998, AstL, 24, 451
Kolotilov, E. A., Shenavrin, V. I., Shugarov, S. Y., & Yudin, B. F. 2003, ARep, 47, 777
Krautter, J. 2008, in Classical Novae, ed. M. F. Bode & A. Evans (Cambridge: Cambridge Univ. Press), 232
Li, K.-L., Chomiuk, L., & Strader, J. 2017a, ATel, 10977, 1
Li, K.-L., Chomiuk, L., & Strader, J. 2018a, ATel, 11590, 1
Li, K.-L., Hambsch, F.-J., Munari, U., et al. 2020, ApJ, 905, 114
Li, K.-L., Metzger, B. D., Chomiuk, L., et al. 2017b, NatAs, 1, 697
Li, K.-L., Mukai, K., Nelson, T., & Chomiuk, L. 2018b, ATel, 11201, 1
Linford, J. D., Chomiuk, L., Nelson, T., et al. 2017, ApJ, 842, 73
Linford, J. D., Ribeiro, V. A. R. M., Chomiuk, L., et al. 2015, ApJ, 805, 136
Luckas, P. 2016, ATel, 9658, 1
Luckas, P. 2017, ATel, 10795, 1
Martin, P., & Dubus, G. 2013, A&A, 551, A37

Mason, E., Shore, S. N., De Gennaro Aquino, I., et al. 2018, ApJ, 853, 27
Metzger, B. D., Caprioli, D., Vurm, I., et al. 2016, MNRAS, 457, 1786
Metzger, B. D., Finzell, T., Vurm, I., et al. 2015, MNRAS, 450, 2739
Metzger, B. D., Hascoët, R., Vurm, I., et al. 2014, MNRAS, 442, 713
Mukai, K., & Ishida, M. 2001, ApJ, 551, 1024
Mukai, K., Orio, M., & Della Valle, M. 2008, ApJ, 677, 1248
Munari, U. 2013, ATel, 4709, 1
Munari, U., Hambsch, F.-J., & Frigo, A. 2017, MNRAS, 469, 4341
Munari, U., Joshi, V. H., Ashok, N. M., et al. 2011, MNRAS, 410, L52
Munari, U., Margoni, R., & Stagni, R. 1990, MNRAS, 242, 653
Munari, U., Moretti, S., & Maitan, A. 2020, A&A, 639, L10
Munari, U., & Ochner, P. 2018, ATel, 11926, 1
Nelson, T., Donato, D., Mukai, K., Sokoloski, J., & Chomiuk, L. 2012, ApJ, 748, 43
Nelson, T., Mukai, K., Li, K.-L., et al. 2019, ApJ, 872, 86
Ness, J.-U., Schwarz, G. J., Retter, A., et al. 2007, ApJ, 663, 505
O'Brien, T. J., Lloyd, H. M., & Bode, M. F. 1994, MNRAS, 271, 155
Orio, M., Covington, J., & Ögelman, H. 2001, A&A, 373, 542
Orlando, S., & Drake, J. J. 2012, MNRAS, 419, 2329
Osborne, J. P. 2015, JHEAp, 7, 117
Osborne, J. P., Page, K. L., Beardmore, A. P., et al. 2011, ApJ, 727, 124
Page, K. L., Beardmore, A. P., & Osborne, J. P. 2020a, AdSpR, 66, 1169
Page, K. L., Kuin, N. P. M., Beardmore, A. P., et al. 2020b, MNRAS, 499, 4814
Page, K. L., & Osborne, J. P. 2014, in ASP Conf. Ser. 490, Stellar Novae: Past and Future Decades, ed. P. A. Woudt & V. A. R. M. Ribeiro (San Francisco, CA: ASP), 345
Page, K. L., Osborne, J. P., Kuin, N. P. M., et al. 2015, MNRAS, 454, 3108
Patterson, J. 1994, PASP, 106, 209
Payne-Gaposchkin, C. H. P. 1957, in The Galactic Novae, ed. I. P. Amsterdam (New York: Dover)
Pretorius, M. L., & Mukai, K. 2014, MNRAS, 442, 2580
Prieto, J. L. 2016, ATel, 9564, 1
Schaefer, B. E. 2018a, MNRAS, 481, 3033
Schaefer, B. E. 2018b, MNRAS, 481, 3033
Schwarz, G. J., Ness, J.-U., Osborne, J. P., et al. 2011, ApJS, 197, 31
Shafter, A. W., Darnley, M. J., Hornoch, K., et al. 2011, ApJ, 734, 12
Shappee, B. J., Prieto, J. L., Grupe, D., et al. 2014, ApJ, 788, 48
Shore, S. N., Augusteijn, T., Ederoclite, A., & Uthas, H. 2011, A&A, 533, L8
Shore, S. N., Mason, E., Schwarz, G. J., et al. 2016, A&A, 590, A123
Shugarov, S., Pavlenko, E., Chochol, D., et al. 2014, in ASP Conf. Ser. 490, Stellar Novae: Past and Future Decades, ed. P. A. Woudt & V. A. R. M. Ribeiro (San Francisco, CA: ASP), 217
Sokoloski, J. L., Luna, G. J. M., Mukai, K., & Kenyon, S. J. 2006, Natur, 442, 276
Sokolovsky, K. V., Aydi, E., Chomiuk, L., et al. 2020a, ATel, 13900, 1
Sokolovsky, K. V., Mukai, K., Chomiuk, L., et al. 2020b, MNRAS, 497, 2569
Stanek, K. Z., Holoien, T. W.-S., Kochanek, C. S., et al. 2018, ATel, 11454, 1
Stanek, K. Z., Kochanek, C. S., Brown, J. S., et al. 2016, ATel, 9538, 1
Stanek, K. Z., Kochanek, C. S., Shields, J. V., et al. 2017, ATel, 10772, 1
Steinberg, E., & Metzger, B. D. 2018, MNRAS, 479, 687
Teyssier, F. 2019, CoSka, 49, 217
The Fermi-LAT collaboration 2020, ApJS, 247, 33
Waagen, E. O. 2014, AAN, 2014, 489
Waagen, E. O., Pearce, A., Otero, S., et al. 2013, CBET, 3732, 3
Wagner, R. M., Dong, S., Bensby, T., et al. 2012, ATel, 4157, 1
Walter, F. M. 2018, ATel, 11298, 1
Walter, F. M., Battisti, A., Towers, S. E., Bond, H. E., & Stringfellow, G. S. 2012, PASP, 124, 1057
Warner, B. 1995, Cataclysmic Variable Stars (Cambridge Astrophysics Series), Vol. 28 (Cambridge: Cambridge Univ. Press), 572
Williams, R. E. 1992, AJ, 104, 725
Wolf, W. M., Bildsten, L., Brooks, J., & Paxton, B. 2013, ApJ, 777, 136
Yaron, O., Prialnik, D., Shara, M. M., & Kovetz, A. 2005, ApJ, 623, 398